Head-on collision of normal shock waves in dusty gases

T. Elperin, G. Ben-Dor, and O. Igra*

The head-on collision of normal shock waves in dusty gases has been investigated numerically, using the modified random-choice method. The results concerning the various flow field properties as well as the waves configuration were compared with those of a pure gas case.

Keywords: *shock waves, dusty gases, random choice method*

Introduction

The head-on collision of two normal shock waves is a classical gas dynamic problem first studied in detail by Glass,[1] Gould,[2] and Nicholl[3] more than thirty years ago. A schematic illustration of the waves configuration in the xt plane and their location at a time before, $t<t_c$, and after, $t>t_c$, the head-on collision time, t_c, are shown in Figures 1(a), (b), and (c), respectively.

Before the head-on collision, two shock waves, S_1 and S_2, propagate, one from left to right and the other from right to left, into a quiescent gas, state 0. Two new thermodynamic states 1 and 2 are obtained behind S_1 and S_2, respectively. After the head-on collision, the incident shock waves reflect back as new shock waves, S_3 and S_4, which now move apart. S_3 propagates toward the oncoming flow of state 1 and changes its properties to a new thermodynamic state, state 3, while S_3 propagates toward the oncoming flow of state 2 and changes its properties to a new thermodynamic state, state 4. States 3 and 4 are separated by a contact surface across which the pressures and the flow velocities are constant, but all the other flow properties—density, temperature, entropy, and so on—are different. The contact surface can move either to the left or to the right depending on the strengths, that is, the Mach numbers, of the incident shock waves, S_1 and S_2.

As we mentioned, the head-on collision of normal shock waves was first solved analytically by Glass.[1] The solution is based on applying the well-known conservation equations for a normal shock wave[4] across each of the two incident shock waves separately while imposing the boundary condition of equal pressures and flow velocities on both sides of the contact surface.

Owing to the fact that in nature shock waves usually do not propagate in a pure medium, the analytical solution of Glass is, unfortunately, insufficient, for its applicability is limited. Alternatively, solutions that account for nonhomogeneous flows, similar to those encountered in reality, must be sought. Only these solutions can be used to simulate interactions of shock waves that might occur in reality when blast waves are generated.

Unfortunately, however, these solutions cannot be purely analytical, for the governing equations are too complicated, and one is forced to use various numerical techniques to solve the flow field under consideration and thereby learn about the interaction of shock waves in nonhomogeneous medium such as humid or dusty gases.

General descriptions of gas-particle suspensions can be found in several articles and books.[5-7] When the gaseous phase is assumed to be perfect, the major difference between the case of a pure gas and that of a dusty gas is the existence of a relaxation zone behind the shock wave in the latter. Theoretically, the relaxation zone is infinite in length, for the equilibrium flow properties (which can be calculated only from the initial conditions) of the suspension are asymptotically approached. However, common practice is to define the length of the relaxation zone as the distance behind the shock wave where the suspension properties have reached values differing by a few percent from the equilibrium properties. The pioneering works of Carrier,[8] Kriebel,[9] and Rudinger,[10] as well as the work of Igra and Ben-Dor,[11] verified the existence of this relaxation zone and identified the parameters affecting it.

Present study

Assumptions

This analysis is based on the following assumptions, which are usually used[4-11] when shock waves propagating into dust gas suspensions are investigated.

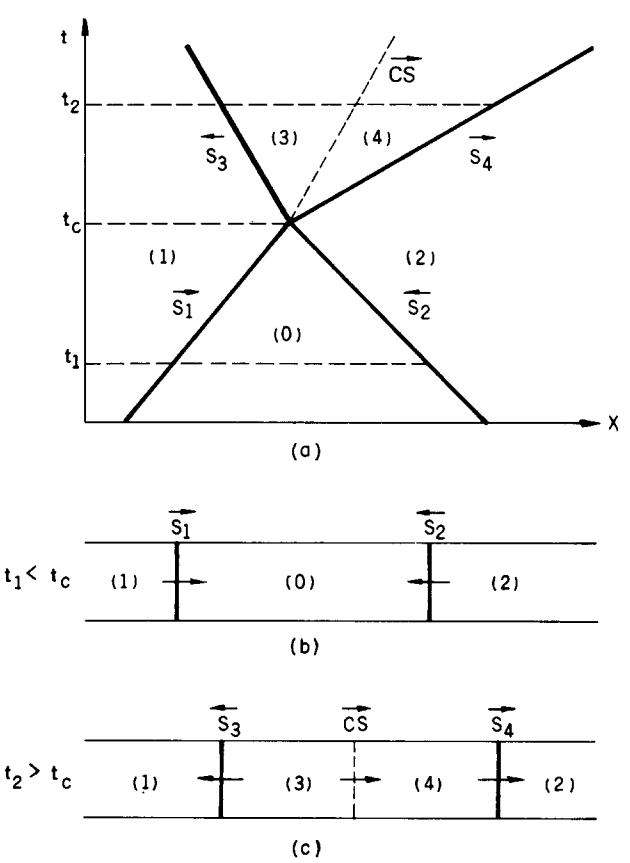

Figure 1 Schematic illustration of the shock waves in the xt plane

* Pearlstone Center for Aeronautical Engineering Studies, Department of Mechanical Engineering, Ben-Gurion University of the Negev, Beer Sheva, Israel

Received 11 July 1986 and accepted for publication 18 March 1987

0142-727X/87/040303-10$03.00

The suspension is assumed to be composed of a thermally perfect inviscid gas and solid particles of spherical shape and uniform diameter. The volume occupied by the solid particles is assumed to be negligible, since the particles' density is greater by orders of magnitude than that of the carrier gas. The gas and the solid particles interact with each other through the drag force, D, and the heat transfer rate, Q. The expressions for D and Q were adopted from Miura and Glass,[12] that is,

$$D=\tfrac{1}{8}\pi d^2\rho(u-v)|u-v|C_D \tag{1a}$$

$$Q=\pi d\mu\frac{C_p}{\mathrm{Pr}}(T-\theta)\,\mathrm{Nu} \tag{1b}$$

where

$$C_D=0.48+28\,\mathrm{Re}^{-0.85}$$

$$\mathrm{Nu}=2.0+0.6\,\mathrm{Pr}^{1/3}\,\mathrm{Re}^{1/2}$$

$$\mathrm{Re}=\frac{\rho|u-v|d}{\mu}$$

$$\mathrm{Pr}=\frac{\mu C_p}{k}$$

In these expressions, u and v are the velocities of the gas and the solid particles; T and θ are the temperature of the gas and the solid particles; d is the diameter of the solid particles; and μ, k, and C_p are the gas dynamic viscosity, thermal conductivity, and specific heat capacity at constant pressure, respectively.

Although the validity of these expressions can be questioned in some cases, the prediction of the suspension properties made on the basis of these expressions was found to be in a reasonably good agreement with results recently obtained in dusty shock tube experiments.[12]

As can be seen from the expression for the drag force, D, the gravity effects, Basset force, and force acting on the solid particles due to pressure gradients are assumed to be negligible. The last assumptions are quite accurate when the solid-gas density ratio is small and pressure gradients are not high.

Besides these assumptions, the gaseous phase is assumed to be a continuous medium with a molecular mean free path much smaller than the size of the solid particles. As we will show, this assumption is valid for the particle diameter used in this study. The effect of compressibility, that is, the dependence of the drag coefficient on the Mach number, can also be neglected for the considered range of flow Mach numbers.[11]

The expression for the heat transfer rate, Q, implies that only convective heat transfer is taken into account. Certainly, when the temperature of the particles becomes high enough, the radiative heat transfer becomes important.[11] Besides the preceding assumptions, it was assumed the temperature within the solid dust particles is uniform. This is true for the case under investigation because the Biot number is greater than 0.1. Finally, it was assumed the concentration of the solid phase is sufficiently low so that the effect of thermal, mechanical, or hydrodynamical interactions between the solid particles can be neglected.

Conservation equations

Under the preceding assumptions, the one-dimensional, nonstationary compressible flow of the gas-dust suspension is governed by the following system of partial differential equations expressing the conservation of mass, momentum, and energy of the gaseous and the solid phases:

$$\frac{\partial\rho}{\partial t}+\frac{\partial}{\partial x}(\rho u)=0 \tag{2}$$

$$\frac{\partial}{\partial t}(\rho u)+\frac{\partial}{\partial x}(\rho u^2+p)=-\frac{\sigma}{m}D \tag{3}$$

$$\frac{\partial}{\partial t}[\rho(C_vT+\tfrac{1}{2}u^2)]+\frac{\partial}{\partial x}[\rho u(C_pT+\tfrac{1}{2}u^2)]=-\frac{\sigma}{m}(vD+Q) \tag{4}$$

$$\frac{\partial\sigma}{\partial t}+\frac{\partial}{\partial x}(\sigma v)=0 \tag{5}$$

$$\frac{\partial}{\partial t}(\sigma v)+\frac{\partial}{\partial x}(\sigma v^2)=\frac{\sigma}{m}D \tag{6}$$

$$\frac{\partial}{\partial t}[\sigma(C_m\theta+\tfrac{1}{2}v^2)]+\frac{\partial}{\partial x}[\sigma v(C_m\theta+\tfrac{1}{2}v^2)]=\frac{\sigma}{m}(vD+Q) \tag{7}$$

where ρ, u, and T are the density, velocity, and temperature of the gaseous phase; and σ, v, and θ are the spatial density, velocity, and temperature of the solid particles.

Numerical technique

This system of partial differential equations was solved numerically by the modified random choice method (RCM) with operator splitting techniques.

The RCM, which represents the combination of the explicit

Notation

a	Local speed of sound of the gaseous phase
C_D	Drag coefficient
C_m	Specific heat capacity of the solid particle
C_p	Specific heat capacity of the gas at constant pressure
C_v	Specific heat capacity of the gas at constant volume
D	Drag force
d	Diameter of the solid particle
k	Thermal conductivity of the gas
L	The distance separating the two incident shock waves at $t=0$
m	Mass of a solid particle
N	Number of mesh points used in the numerical calculations
Nu	Nusselt number
Pr	Prandtl number of the gas
p	Suspension pressure
Q	Heat transfer rate
Re	Reynolds number
S_i	Shock wave inducing a flow state (i) behind it
T	Temperature of the gaseous phase
t	Time coordinate
t_c	Collision time
u	Velocity of the gaseous phase
v	Velocity of the solid phase
x	Spatial coordinate
β	Loading ratio of the solid phase in the suspension
γ	Specific heat capacities ratio of the gas $=\frac{C_p}{C_v}$
θ	Temperature of the gaseous phase
μ	Dynamic viscosity of the gas
ρ	Density of the gaseous phase
ρ_s	Material density of the solid particle
σ	Spatial density of the solid particle
τ	Nondimensionalized time

Subscripts

0	Flow state between the two incident shock waves before their head-on collision
1	Flow state generated by S_1
2	Flow state generated by S_2
3	Flow state generated by S_3
4	Flow state generated by S_4

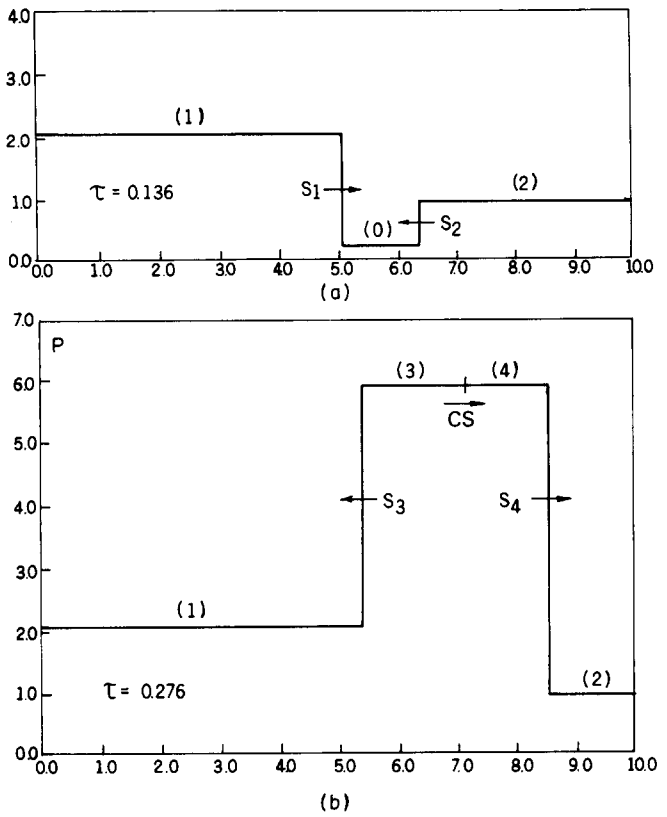

Figure 2 The pressure history before (a) and after (b) the head-on collision for a pure perfect gas ($r=1.4$)

first-order finite difference scheme[13] and the Monte Carlo Method, has been used extensively in recent years in gasdynamics.[12,14] However, the random choice scheme used in this research comprises some modifications that considerably improve the quality of the results. The main advantage of the RCM over other numerical schemes is that it allows high resolution of shock waves and contact surfaces, whereas in other finite difference methods, they are usually smeared over many grid points as a consequence of artificial viscosity and truncation error of the scheme. The RCM uses the exact solution of the Riemann problem with piecewise constant initial data for a finite difference solution of the hyperbolic equations of gasdynamics. The Riemann problem is solved repeatedly between each pair of neighboring spatial grid points. The successive positions of the discontinuities (for example, shock waves) between these mesh points are sampled with the help of the uniformly distributed sequences of Van der Corput.[15] This implementation of uniformly distributed sequences considerably reduces the numerical noise and thus improves the quality of the results (for more details see Reference 15).

Some other important details of the random choice scheme applied in the calculations are as follows. The solution of the Riemann problem with piecewise constant initial data was performed by the iterative method suggested first by Godunov.[13] The homogeneous part of Equations 2–7 was solved by the RCM. The solution is obtained by solving alternately in each time step the two systems of differential equations. The first system of partial differential equations is derived from Equations 2–7, with the right-hand side omitted, and is solved with the RCM. The second system of equations is derived from Equations 2–7 by omitting the spatial derivatives. The resulting system of ordinary differential equations is then solved with the initial data obtained from the random choice solution. In the calculations, the transmissive boundary conditions were assumed for the gaseous phase and the solid phase.

The initial value problem with piecewise constant initial data for Equations 5–7, describing the flow of the solid particles, was treated analytically,[12] assuming a linear distribution of the flow variables between adjacent grid points. This approach allows one to preserve the first-order accuracy of the method and avoids the difficulties arising as a result of the multivalued solution of Equations 5–7.

All the thermodynamic and dynamic variables in Equations 1–7 were nondimensionalized in the following way:

$$\bar{p}=\frac{p}{p_0} \qquad \bar{\rho}=\frac{\rho}{\rho_0} \qquad \bar{\sigma}=\frac{\sigma}{\sigma_0}$$

$$\bar{u}=\frac{\sqrt{\gamma}u}{a_0} \qquad \bar{v}=\frac{\sqrt{\gamma}v}{a_0}$$

$$\bar{T}=\frac{T}{T_0} \qquad \bar{\theta}=\frac{\theta}{T_0}$$

$$\tau=\frac{a_0 t}{\sqrt{\gamma}L} \qquad \bar{X}=\frac{x}{L}$$

where subscript 0 refers to the flow state originally separating the two oncoming incident shock waves (S_1 and S_2 in Figure 1a), and L is a characteristic length (the separation between the two incident shock waves at $t=0$). All the calculations were performed with $N=750$ mesh points. The average running time was 1200 seconds CPU on the CDC Cyber 180-840 computer.

Results and discussions

Pure gas

As a first step, the computer code developed for solving the problem at hand was checked by comparing its predictions for the classical case of the head-on collision of two normal shock

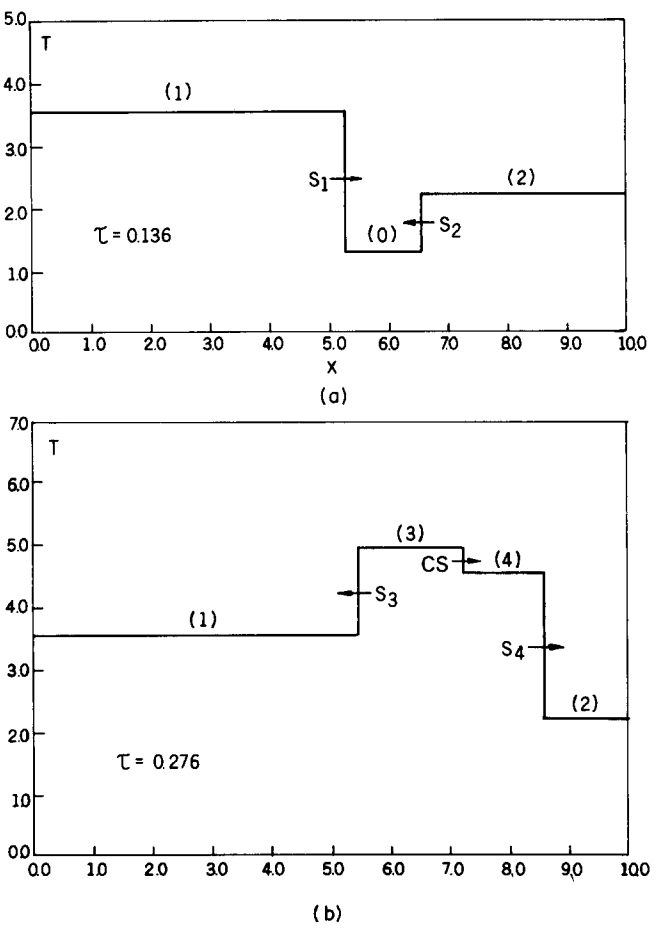

Figure 3 The temperature history before (a) and after (b) the head-on collision for a pure perfect gas ($r=1.4$)

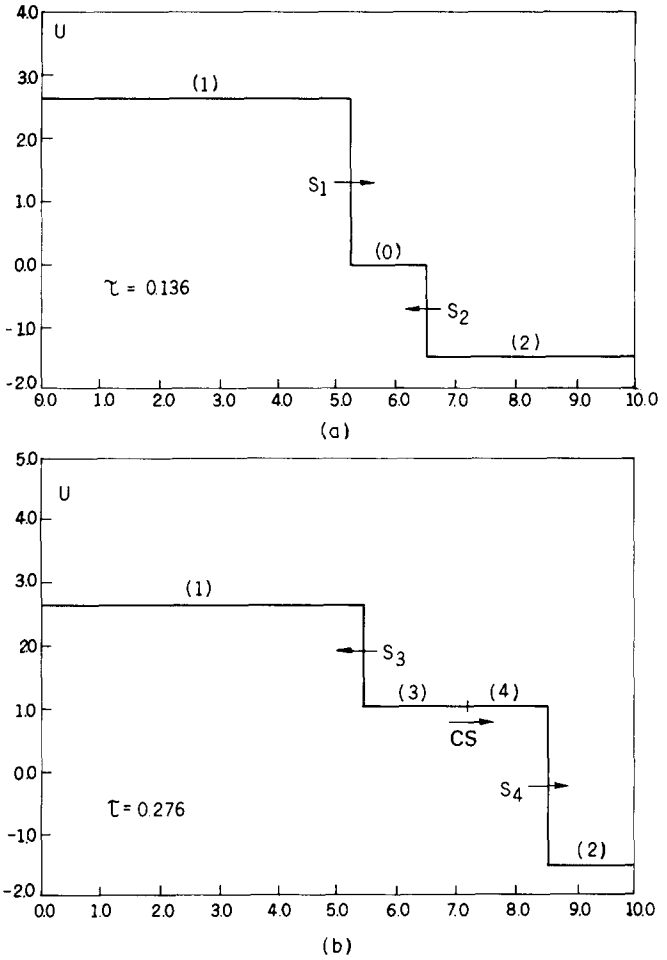

Figure 4 The velocity history before (a) and after (b) the head-on collision for a pure perfect gas ($r=1.4$)

waves in a pure gas with the results predicted analytically by Glass[1] for identical initial conditions. Excellent agreement was obtained.

Typical results for the pressure, temperature, and gas velocity are shown in Figures 2, 3, and 4, respectively. Each of these figures consists of two parts: before and after the head-on collision. The Mach number of the shock wave propagating from left to right is 3, and that of the shock wave propagating from right to left is 2. In Figure 2(a), the two shock waves, S_1 and S_2, can be seen to propagate one toward the other. The sharp pressure jump across each of them clearly indicates the effectiveness of the modified RCM in describing shock waves. Figure 2(b) shows the pressure history after the head-on collision. The pressure jumps across the S_3 and S_4 shock waves are again seen to be very sharp. Since $P_3=P_4$, the contact surface (CS) separating states 3 and 4 in Figure 1(a) cannot be identified in the pressure plot.

Figure 3(a) illustrates the temperature profile before the head-on collision. The sharp jumps across S_1 and S_2 are again clearly seen. In Figure 3(b), where the temperature profile after the head-on collision is shown, a contact surface between states 3 and 4 is clearly seen. For the incident shock wave Mach numbers chosen for the case at hand, T_3 is greater than T_4.

The shock-induced flow velocities behind S_1 and S_2 are shown in Figure 4(a). The flow behind S_1 moves to the right, so u_1 is positive, whereas the flow behind S_2 moves to the left, so u_2 is negative. After the head-on collision (Figure 4b), the flow velocities in both sides of the contact surface, which are equal (that is, $u_3=u_4$), are positive. Hence the resulted contact surface, which has the same velocity as the two flow states in either side of it, is following the S_4 reflected shock wave that is moving to the right. Because of the boundary condition of equal flow velocities in both sides of the contact surface, it cannot be identified in the velocity plot.

Moreover, since the gas under consideration is a perfect pure gas, the values of the flow properties behind the shock waves remain constant and both the incident and reflected shock waves propagate with constant velocities. Only the distances between the various discontinuities are changing linearly with time.

Dusty gas

The results presented are for the same incident shock waves, that is, the identical Mach numbers, used earlier to illustrate the head-on collision in pure gases. The loading ratio of the solid particles (dust) is $\beta=1$, the diameter of each dust particle is $d=10^{-5}$ m, and its material density is $\rho_s=2.5$ gm/cm^3. The two shock waves were originally separated by a distance L and started propagating one toward the other at $\tau=0$. Figure 5(a) illustrates the pressure histories for five different times: $\tau=0.036$, 0.076, 0.116, 0.156, and 0.196, all of which correspond to situations where the two shock waves are propagating one toward the other before their head-on collision (Figure 2a). Unlike the previous case where, throughout the entire jump, the shock wave fronts were sharp, here only a small portion of shock wave fronts is sharp. The sharp front is then followed by a further increase in the pressure to a maximum value, after which a gradual decrease in the pressure is visible. The sharp portion of the shock waves is decreasing with time as the shock waves propagate. This clearly indicates that the dust presence causes the shock waves to decelerate; however, the maximum pressure obtained behind them increases, but it takes a longer time for the pressure to reach its maximum value. This fact suggests the shock waves become more and more dispersed as they continue propagating in the dusty medium.

Figures 5(b) and 5(c) represent the pressure distribution in the flow field for nine different times, namely, $\tau=0.216$, 0.236, 0.256, 0.276, 0.296, 0.316, 0.336, 0.356, and 0.376. The first five cases are shown in Figure 5(b), and the last five cases are shown in Figure 5(c). All the distributions correspond to times after the head-on collision. For the first four cases ($\tau=0.216$, 0.236, 0.256, and 0.276), the pressure behind the two reflected shock waves resembles a spikelike shape that first increases in its maximum and then, as the shock waves move farther away, starts to decay. While the S_3 shock seems to be accelerating (it moves longer distances in the same time intervals as time goes on), the S_4 shock is almost stationary until about $\tau=0.276$, after which its propagation to the left becomes evident.

The sequence shown in Figure 5(b) continues in Figure 5(c). For clarity, the pressure profile for $\tau=0.296$ appears in both Figures 5(b) and 5(c). The spike in the pressure behind the two shock waves obtained immediately after the head-on collision is seen to be smeared out at a later time. Instead, a local minimum in the pressure is obtained between the two reflected shock waves. Although both shock waves seem to propagate at almost constant velocities, the decreasing maximum pressure jump across them clearly suggests the reflected shock waves are slowing down with time. Moreover, the shock fronts after the head-on collision seem to be much sharper than those before the collision. This might be because the reflected shock waves propagate into nonuniform suspensions.

The gas temperature, T, in the flow field for five different times before the shock waves head-on collision and for five different times after the head-on collision are shown in Figures 6(a) and 6(b), respectively. Unlike the pressure profiles shown earlier, where a sharp increase followed by a further gradual increase was obtained, the gas temperature rise across the incident shock waves resembles a double-step type rise (see Figure 6a). The maximum temperature behind the shock wave increases as time goes on and then gradually decreases.

Immediately after the head-on collision ($\tau=0.216$ in Figure 6b), the temperature profile also resembles a spikelike shape, but only for a short time. As the two reflected shock waves move away and interact with the oncoming flows, which as mentioned

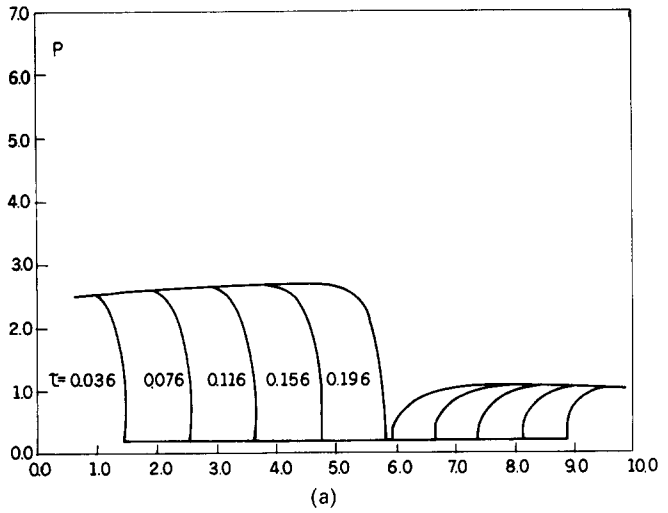

(a)

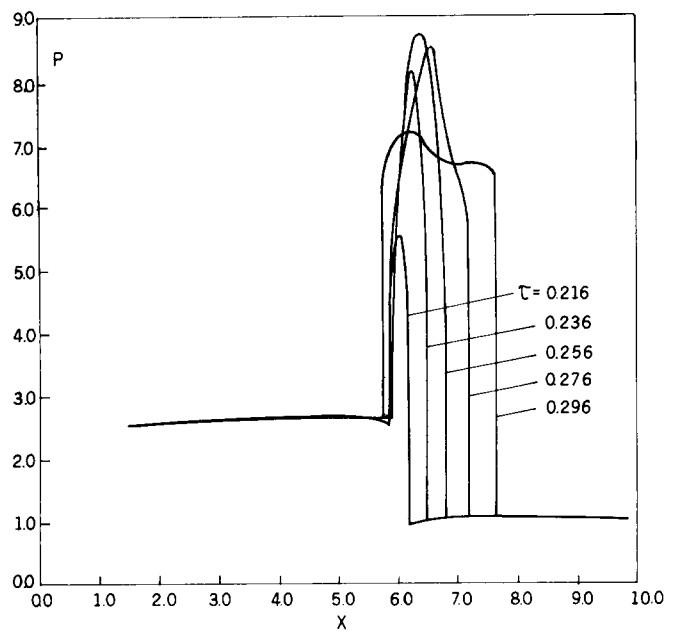

(b)

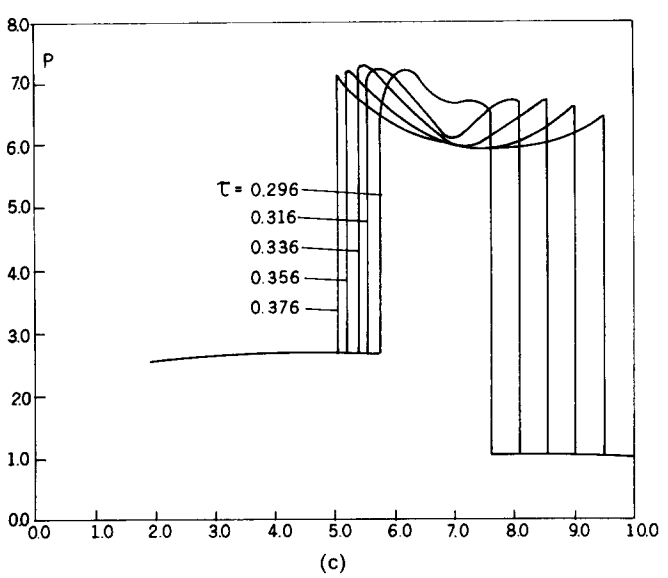

(c)

Figure 5 (a) Pressure histories in a dusty gas for five different times before the head-on collision; (b) pressure histories in a dusty gas for five different times shortly after the head-on collision; (c) pressure histories in a dusty gas for five different times long after the head-on collision

earlier, have a double-step shape temperature profile, the temperature spike is quickly smeared out. Instead, the temperature profile is seen to sharply rise at the fronts of the reflected shock waves S_3 and S_4. The sharp rise in the gas temperature at the shock waves fronts is followed by a gradual decrease in the gas temperature, which changes into a sharp decrease farther away from the shock fronts. The large gap generated by this sudden decrease in the temperatures probably indicates the location of the "contact surface," which for the case of a dusty gas, is not an ideal infinitely thin interface anymore, but a contact region in which the flows generated by S_3 and S_4 are mixed and exchange momentum and energy. Again, while S_3 is seen to be accelerating, S_4 is almost stationary at early times after the head-on collision; S_4 does, however, start to accelerate at later times.

The gas velocity profiles, u, before and after the head-on collision are seen in Figures 7(a) and 7(b), respectively. In Figure 7(a), the gas velocity is seen to sharply rise at the shock fronts. The sharp rise is then followed by a further gradual increase. The gas behind S_1 is moving from left to right, so u_1 is positive, whereas the gas behind S_2 is moving from right to left, so u_2 is negative. After the head-on collision (Figure 7b), the flow between the two reflected shock waves, in states 3 and 4, is positive; hence, it follows the S_4 reflected shock wave. As time goes on, the gas velocity between the two shock waves approaches almost a uniform value. Note also the sharp rise in

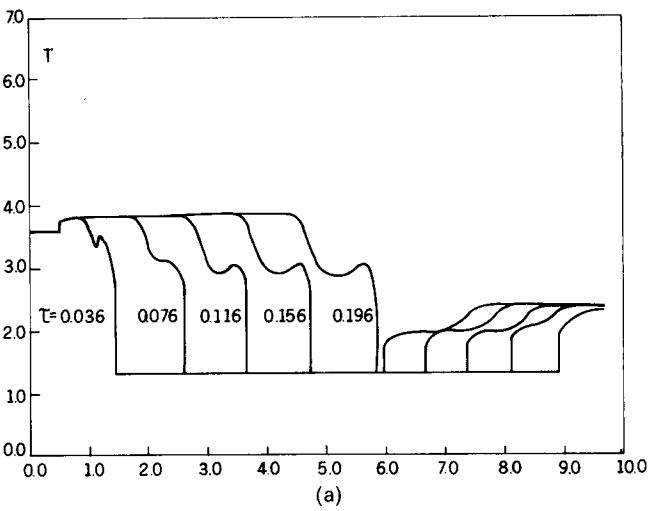

(a)

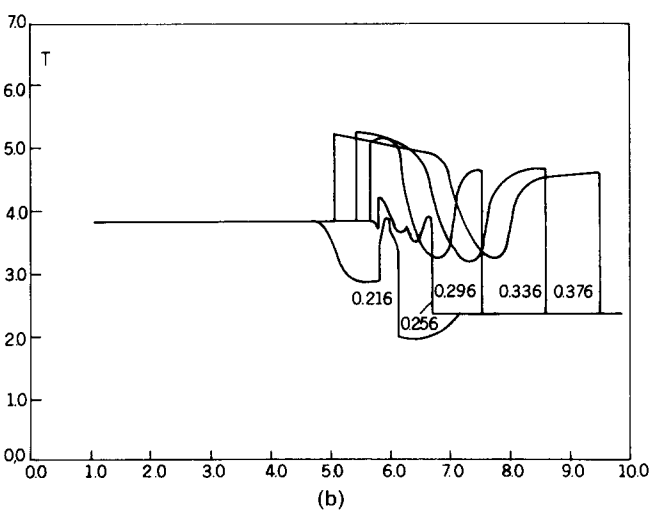

(b)

Figure 6 (a) Gas temperature histories in a dusty gas for five different times before the head-on collision; (b) gas temperature histories in a dusty gas for five different times after the head-on collision

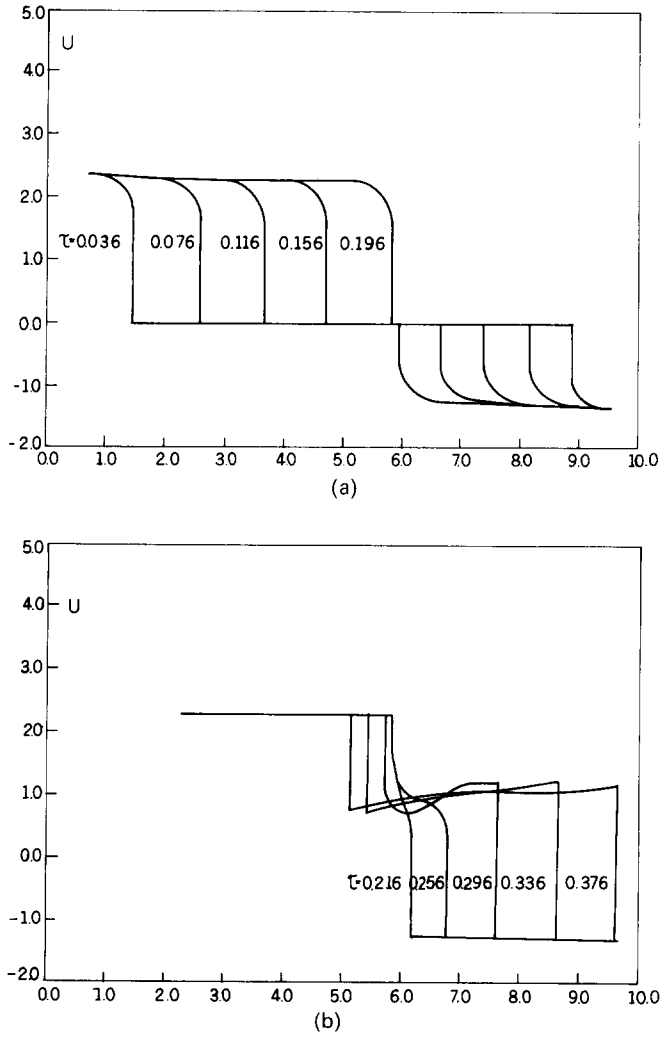

Figure 7 (a) Gas velocity histories in a dusty gas for five different times before the head-on collision; (b) gas velocity histories in a dusty gas for five different times after the head-on collision

the gas velocities across the reflected shock waves as they propagate toward the oncoming nonuniform flows in states 3 and 4. These sharp rises, which are obtained even though the reflected shock waves propagate into dusty-gas suspensions, might be due to the nonuniformity of the flow fields ahead of them. Recall that the shape of the velocity rise across the incident shock waves that propagate into uniform dusty-gas suspensions was much different (see Figure 7a). Unlike the temperature profiles, Figures 5(c) and 6(b), where a contact mixing region betwen the reflected shock waves, S_3 and S_4, was quite evident, here there is no indication of such a region, probably because of the very effective momentum exchange between the two phases.

The properties of the solid particles, namely, temperature, velocity, and spatial density will next be discussed. It should be clarified that the initial condition of the problem at hand was a situation in which two incident shock waves start to propagate into a quiescent gas seeded with solid particles. Since both shock waves induce behind them two flow fields that follow them, respectively, the dust particles encountered by the incident shock waves are first swept toward the point where the two incident shock waves collide head-on. Therefore, in the following flow profiles, the location of the profiles' two edges changes with time.

Figure 8(a) shows the temperature profile of the solid particles, θ, at five different times before the head-on collision. At early times (for example, $\tau = 0.036$), a gradual increase in the particle temperature is seen behind the incident shock waves. However, as times goes on (for example, $\tau = 0.196$), the temperature profile changes into a double-step shape. Moreover, the maximum temperature of the solid particles behind the incident shock waves increases as time goes on.

Figure 8(b) shows the temperature profile of the solid particles after the head-on collision. The arrows on the vertical lines of each profile indicate the direction of propagation of the edge of the dust clouds. Up to a time of about $\tau = 0.256$, the right edge of the dust cloud propagates from right to left; at a later time, $\tau = 0.296$, it assumes an opposite direction.

The velocity profiles of the solid particles, v, before and after the head-on collision are shown in Figures 9(a) and 9(b), respectively. As the incident shock waves propagate (see Figure 9a), their fronts become more and more sharp. The velocity profiles after the head-on collision (Figure 9b) indicate that when the interaction of the two oncoming shock-induced flows is completed, the entire flow between the two reflected shock waves moves to the right. The flow between the two reflected shock waves is again seen to assume quite a uniform state, again suggesting a very efficient momentum exchange.

The earlier mentioned sweeping process of the dust cloud toward the point of the head-on collision is clearly seen in Figure 10(a), where the dust spatial density profiles, σ, at five different times before the head-on collision are seen. As the incident shock waves propagate one toward another, more dust is enclosed between them and the respective edges of the dust

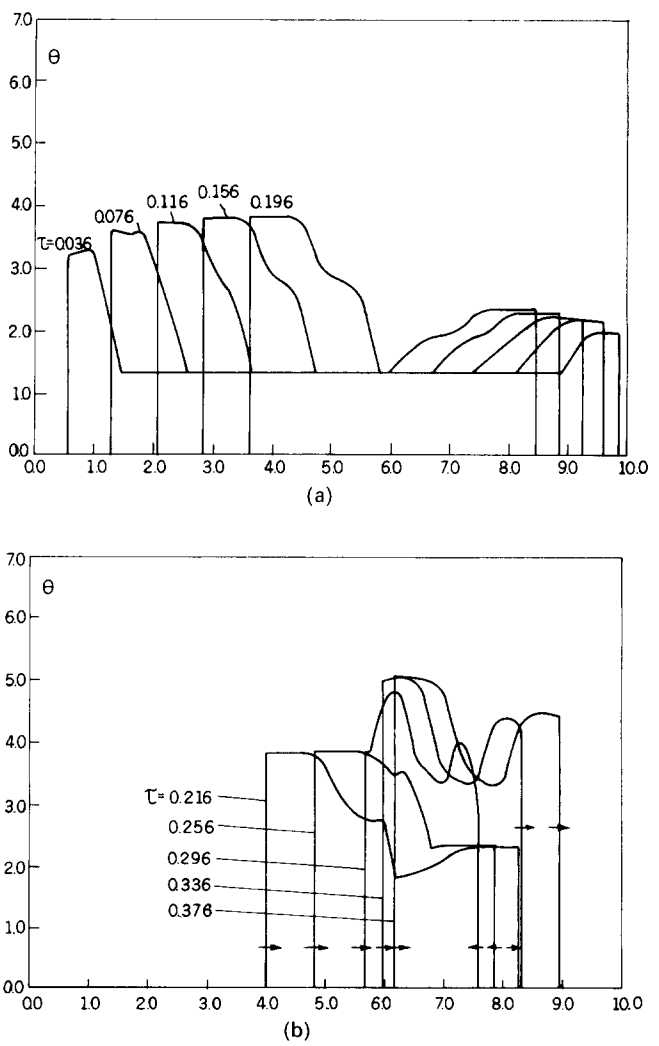

Figure 8 (a) Dust temperature histories in a dusty gas for five different times before the head-on collision; (b) dust temperature histories in a dusty gas for five different times after the head-on collision

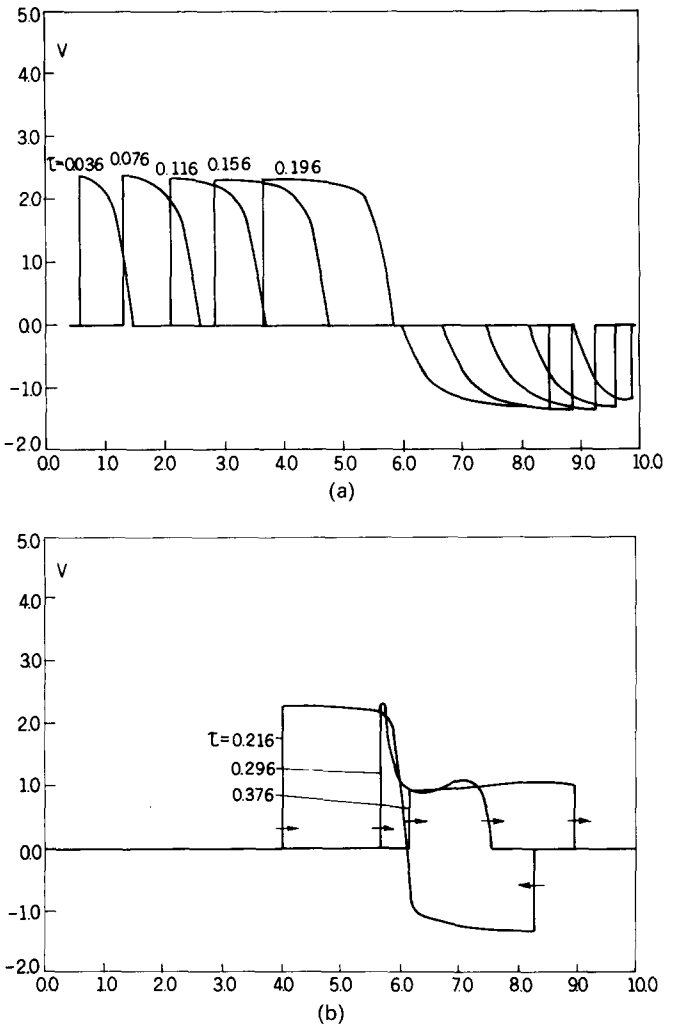

Figure 9 Dust velocity histories in a dusty gas for five different times before the head-on collision; (b) dust velocity histories in a dusty gas for five different times after the head-on collision

cloud. This, in turn, results in a greater maximum in the local spatial density. The spatial density, σ, shortly after the head-on collision when the two shock-induced flows are still flowing one toward another, is seen in Figure 10(b) for $\tau = 0.216$. At a later time, after the interaction of the two shock-induced flows is completed and the entire flow moves to the right, the profile of the spatial density of the solid particles develops a spikelike shape. As the dust cloud is swept to the right (that is, as τ increases), the local maximum in the spatial density decreases, and the dust cloud widens (compare $\tau = 0.296$ and $= 0.376$).

The temperature profiles of the gas and solid particles at four different times are shown in Figures 11(a)–(d). Figure 11(a) corresponds to a time before the head-on collision. The solid line represents the gas temperature, and the dashed line the solid particles temperature. Unlike the gas temperature that rises sharply at the incident shock wave fronts, the solid particles temperature rises much more slowly. However, behind the incident shock wave, the solid particles temperature reaches that of the gas, and the suspension reaches thermal equilibrium. Figure 11(b) corresponds to a time just after the head-on collision ($\tau = 0.216$). Again, it is seen that the solid particles temperature lags behind that of the gas at the reflected shock fronts, which are moving apart, while the suspension is in a thermal equilibrium farther downstream.

At a later time, $\tau = 0.276$, the solid particles temperature profiles start to catch up with that of the gas, and two temperature spikes start to develop accordingly (Figure 11c). At this instant, the two reflected shock waves are still propagating inside the dust cloud (dashed vertical lines).

Figure 11(d) corresponds to a time when the reflected shock waves have emerged from the dust cloud enclosed between the two dashed vertical lines. At this late time ($\tau = 0.356$), the solid particles temperature has already reached a state of thermal equilibrium with the gas.

The velocity profiles of the gas and dust particles are similarly compared in Figures 12(a)–(c). Before the head-on collision (Figure 12a), it is seen that the solid particles reach a kinematic equilibrium with the gas at some distance behind the incident shock fronts. The comparison between the velocity profiles for a time after the head-on collision ($\tau = 0.276$) is shown in Figure 12(b). While the entire gaseous phase is already moving to the right, part of the solid phase, namely, that induced by the S_2 incident shock wave, is still moving to the left. The momentum exchange reverses the direction of propagation of the solid dust that was still propagating to the left at $\tau = 0.276$, and at a later time, $\tau = 0.356$, the entire suspension propagates from left to right. Figure 11(c), which corresponds to this situation, indicates that the velocity of the dust particles has reached the gas velocity and, hence, the suspension is in a state of kinematic equilibrium. It was shown earlier (Figure 11d) that at this late time ($\tau = 0.356$), the suspension has also reached a thermal equilibrium. Thus the entire suspension is in a state of thermodynamic equilibrium.

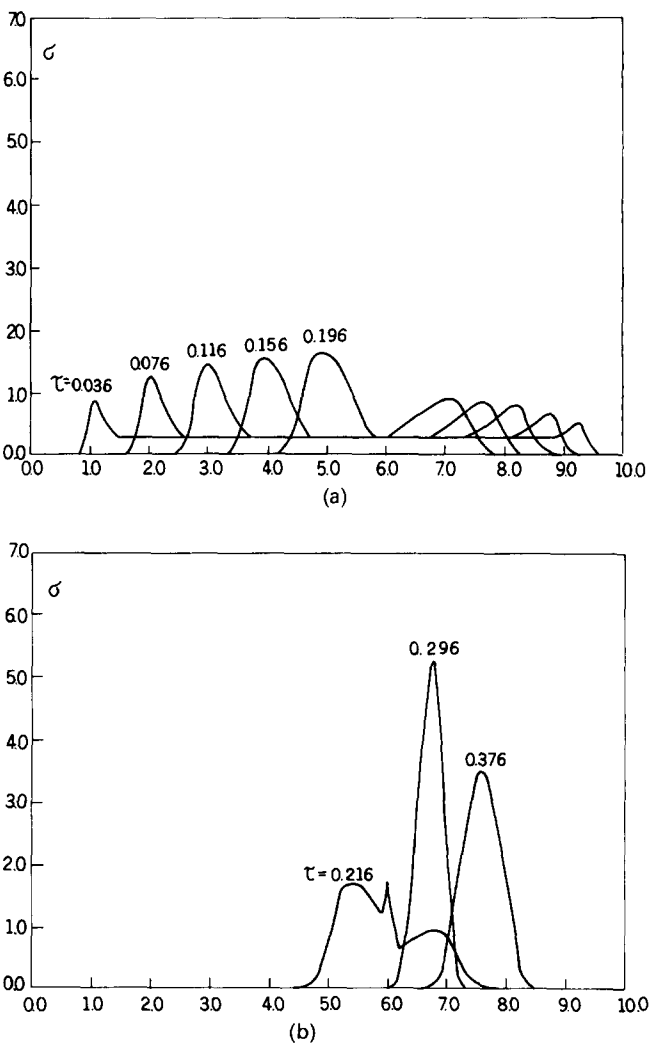

Figure 10 (a) Dust spatial density histories in a dusty gas for five different times before the head-on collision; (b) dust spatial density histories in a dusty gas for five different times after the head-on collision

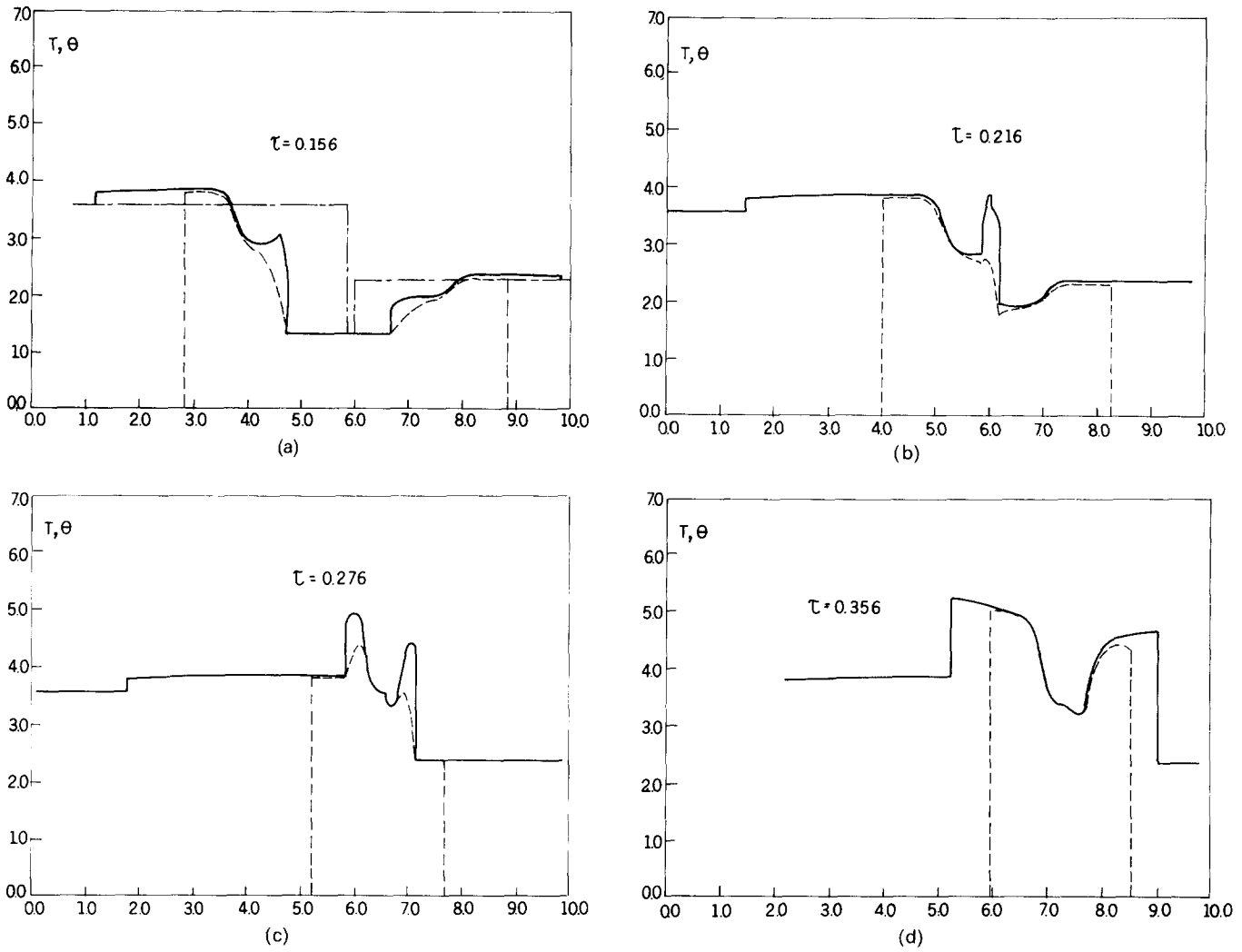

Figure 11 Comparison between the gas and dust temperatures for a pure and dusty gas: (a) before the head-on collision; (b) immediately after the head-on collision; (c) after the head-on collision (before the emergence of the reflected shock waves from the dust cloud); (d) after the head-on collision (after the emergence of the reflected shock waves from the dust cloud)

Comparison between pure and dusty gases

The dashed-dotted lines in Figures 11(a) and 12(a) represent the gas temperature and gas velocity profiles for a dust-free gas. It is evident from Figure 12(a) that the incident shock waves propagate much faster in a pure gas. At $\tau = 0.156$, they have almost collided when the gas is dust free, whereas they are still farther away when the gas is seeded with solid particles.

Moreover, Figure 11(a) indicates that higher temperatures are obtained behind the shock waves when the gas is seeded with dust particles. The higher temperatures may be because the gas velocities of a dusty gas are smaller than those of a pure gas (see Figure 12a). Thus it is possible that part of the kinetic energy released when the gaseous phase is slowed down by the solid phase is transformed into thermal energy.

The pressure distributions in the flow field at three different times are shown in Figures 13(a)–(c). Figure 13(a), which corresponds to a time before the head-on collision, $\tau = 0.156$, indicates that the pressures obtained behind the incident shock waves in the case of a dusty gas are higher than those appropriate to a pure gas. At early times after the head-on collision (Figure 13b), the pressure in the case of a dusty gas yields a very high spike, contrary to the flat shape of the pressure for the case of a dust-free gas. The peak pressure in the case of a dusty gas is almost 50% higher than that appropriate to a pure gas at the same time after the head-on collision. At a later time (Figure 13c), the spike in the pressure is smeared out, and the pressures between the two reflected shock waves approach both the magnitude and the shape of those obtained in the case of a dust-free gas. The dashed-dotted line in Figure 13(c) corresponds to the pressures appropriate to the case of a pure gas (compare the pressure profiles at $\tau = 0.396$). The dashed line in Figure 13(c) represents the constant value of the pressure between the two reflected shock waves for the case of a pure gas.

Conclusion

The head-on collision of two normal incident shock waves in a dusty-gas suspension has been investigated numerically. As a first step, the governing equations of the flow field at hand were developed for the assumptions of the present model. Then they were solved numerically using the modified RCM. Profiles of the various suspension properties, namely, the temperatures, velocities, spatial densities of the gaseous and solid phases, as well as the suspension pressure, were obtained for a variety of times before and after the head-on collision.

Besides the well-known fact that the incident shock waves slow down because of the presence of the dust, it was observed that the reflected shock waves propagate more slowly in a dusty gas. The sudden change in the suspension properties across the reflected shock waves was found to be much more sharp than across the incident shock waves. This was because while the incident shock waves propagate into a uniform dusty gas, the reflected shock waves propagate into a nonuniform suspension.

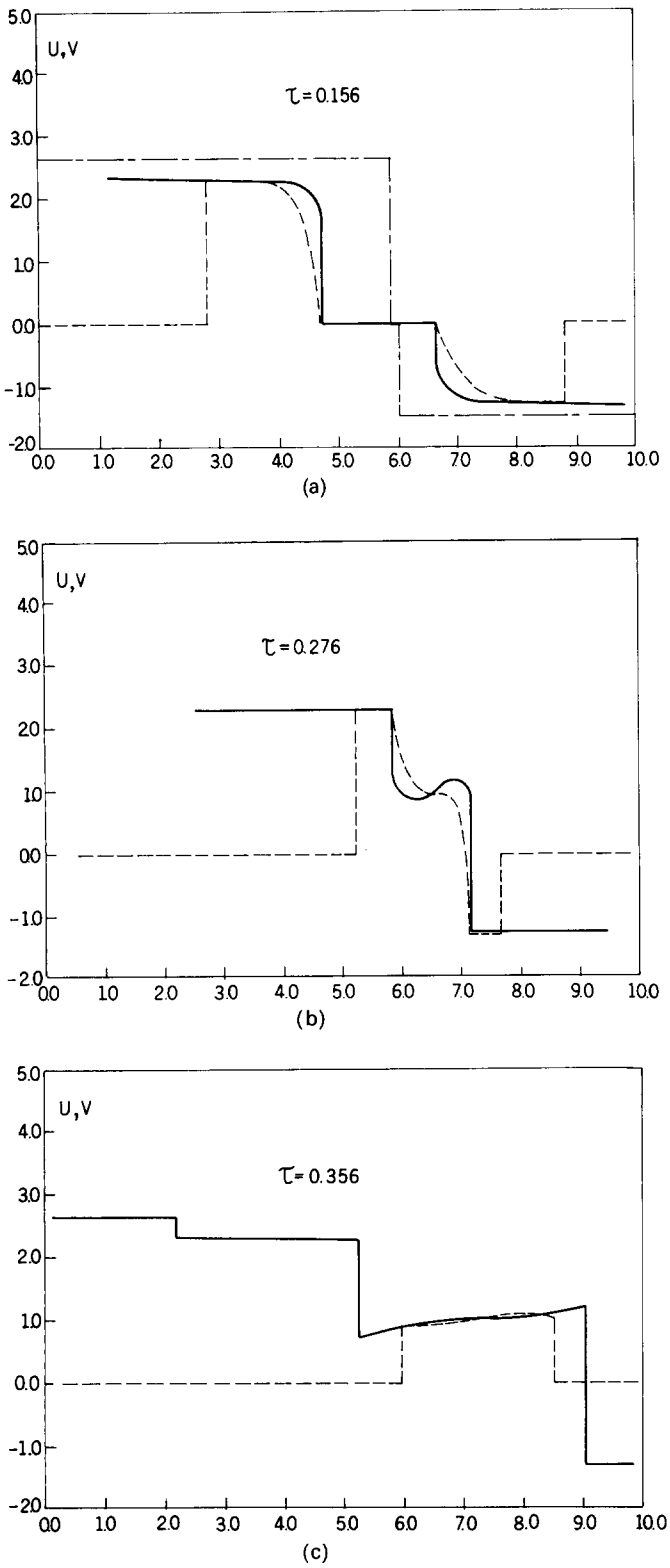

Figure 12 Comparison between the gas and dust velocities for a pure and a dusty gas: (a) before the head-on collision; (b) after the head-on collision (before relaxation); (c) after the head-on collision (after relaxation)

The relaxation process behind the various shock waves was also observed as the temperatures and velocities of the gaseous and solid phases were seen to approach each other far behind the shock fronts.

It should be mentioned finally that Miura *et al.*[16] have recently studied the case of the reflection of a normal planar shock wave from a rigid wall in a dusty gas. Their study is a private case of the more general case investigated in this study,

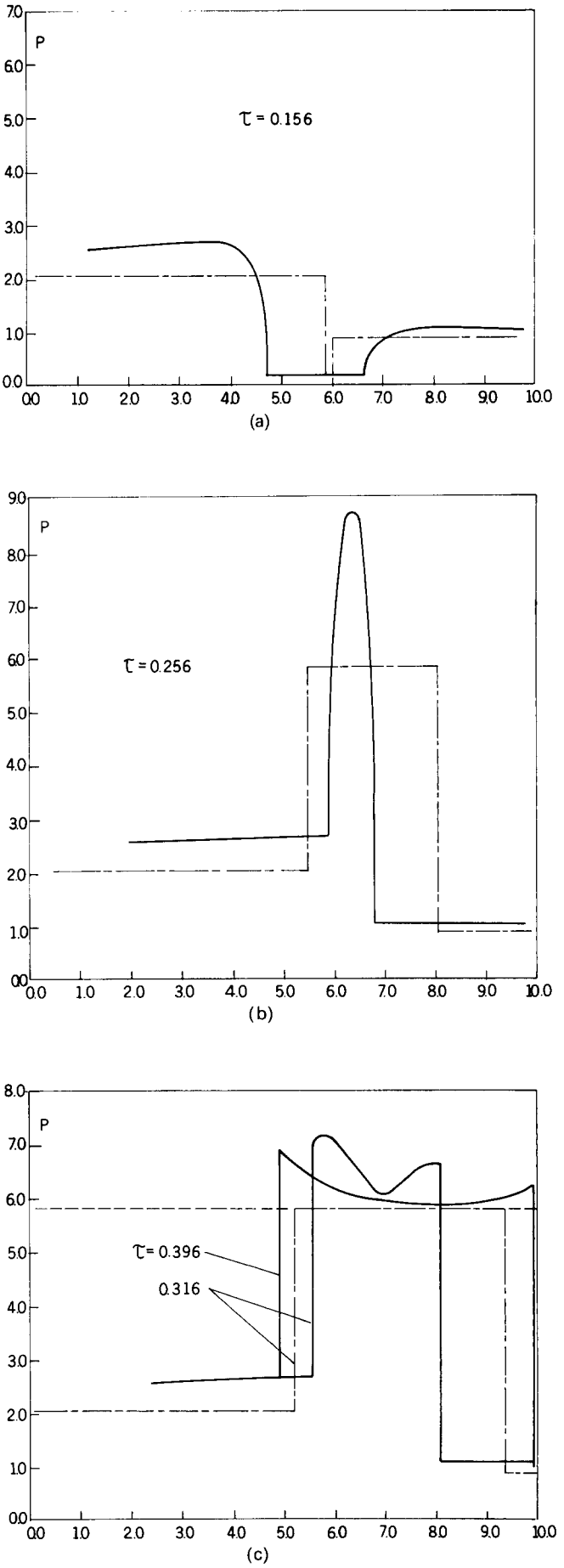

Figure 13 Comparison between the pressures for a pure and a dusty gas: (a) before the head-on collision; (b) immediately after the head-on collision; (c) long after the head-on collision

for it is identical to the head-on collision of two incident shock waves having identical strengths.

References

1 Glass, I. I. Private communication, 1987

2 Gould, D. G. The head-on collision of two shock waves and a shock and rarefaction wave in one-dimensional flow. UTIAS review no. 17, 1952.

3 Nicholl, C. I. H. The head-on collision of shock and rarefaction waves. UTIAS report no. 10, 1951.

4 Anderson, J. N. *Modern Compressible Flow*. McGraw-Hill, New York, 1982.

5 Soo, S. L. *Fluid Mechanics of Multiphase Systems*. Blaisdell Publishing, Waltham, Massachusetts, 1967.

6 Marble, F. E. Dynamics of dusty gases. *Ann. Rev. Fluid Mech.*, 1970, **2**, 397–446.

7 Rudinger, G. Wave propagation in suspension of solid particles in gas flow. *Appl. Mech. Rev.* 1973, **26**, 273–279.

8 Carrier, G. F. Shock waves in dusty gases. *J. Fluid Mech.*, 1958, **4**, 376–382.

9 Kriebel, A. R. Analysis of normal shock waves in a particle laden gas. *J. Basic Eng., Trans. ASME*, ser. D86, 1964, 655–663.

10 Rudinger, G. Some properties of shock relaxation in gas flow carrying small particles. *Phys. Fluids*, 1964, **7**, 658–663.

11 Igra, O., and Ben-Dor, G. Parameters affecting the relaxation zone behind normal shock waves in a dusty gas. *Israel J. Tech.*, 1980, **18**, 159–168.

12 Miura, H., and Glass, I. I. On the passage of a shock wave through a dusty layer. *Proc. Royal Soc. London*, ser. A, 1983, **385**, 85–105.

13 Godunov, S. K. Finite difference method for numerical calculations of discontinuous solutions of equations of hydrodynamics. *Math. Sbornik*, 1959, **47**, 271–306.

14 Saito, T., and Glass, I. I. Applications of random choice method to problems in gasdynamics. *Prog. Aero. Sci.*, 1984, **21**, 201–247.

15 Elperin, T., and Igra, O. About the choice of uniformly distributed sequences to be used in the random choice method. *Comp. Methods Appl. Mech. and Eng.*, 1986, **57**, 181–189.

16 Miura, H., Saito, T., and Glass, I. I. Shock-wave reflection from a rigid wall in a dusty gas. *Proc. Royal Soc. London*, ser. A, 1986, **404**, 55–67.